Unclassified

SECURITY CLASSIFICATION OF THIS PAGE

(2)

REPORT DOCUMENTATION PAGE

1a. REPORT SECURITY CLASSIFICATION: Unclassified	1b. RESTRICTIVE MARKINGS: None
2a. SECURITY CLASSIFICATION AUTHORITY	3. DISTRIBUTION/AVAILABILITY OF REPORT: Approved for public release; distribution unlimited.
2b. DECLASSIFICATION/DOWNGRADING SCHEDULE	
4. PERFORMING ORGANIZATION REPORT NUMBER(S)	5. MONITORING ORGANIZATION REPORT NUMBER(S): AFOSR-TR- 91 0453
AD-A234 699	
6a. NAME OF PERFORMING ORGANIZATION: University of Pennsylvania	6b. OFFICE SYMBOL (If applicable):
6c. ADDRESS (City, State and ZIP Code): Dept of Matl's Sci & Eng, Philadelphia PA 19104	7a. NAME OF MONITORING ORGANIZATION: Department of Air Force - AFOSR
	7b. ADDRESS (City, State and ZIP Code): Department of Air Force - AFOSR, Bolling Air Force Base, Washington, DC 20332-6448
8a. NAME OF FUNDING/SPONSORING ORGANIZATION: AFOSR	8b. OFFICE SYMBOL (If applicable): NE
	9. PROCUREMENT INSTRUMENT IDENTIFICATION NUMBER: AFOSR 89-0062
8c. ADDRESS (City, State and ZIP Code): Department of Air Force - AFOSR, Bolling Air Force Base, Washington, DC 20332-6448	10. SOURCE OF FUNDING NOS.

PROGRAM ELEMENT NO.	PROJECT NO.	TASK NO.	WORK UNIT NO.
61102F	2306	A1	

11. TITLE (Include Security Classification): Plasticity of Single Crystalline Al_3X Intermetallic Compounds

12. PERSONAL AUTHOR(S): David Luzzi, David Pope, Vaclav Vitek

13a. TYPE OF REPORT	13b. TIME COVERED	14. DATE OF REPORT (Yr., Mo., Day)	15. PAGE COUNT
~~Intermediate~~ Annual	FROM 7/3/90 TO 3/31/91	4/6/91	16

16. SUPPLEMENTARY NOTATION

17. COSATI CODES			18. SUBJECT TERMS (Continue on reverse if necessary and identify by block number)
FIELD	GROUP	SUB. GR.	

19. ABSTRACT (Continue on reverse if necessary and identify by block number)

This report summarizes our progress on this program in three areas: Deformation of $L1_2$ single crystalline Al_3Ti + Fe, high resolution transmission electron microscopy of dislocations and faults in this material, and computer simulations of dislocations and faults in both the DO_{22} and $L1_2$ form. The slip systems have been determined from macroscopic and microscopic analysis, and a new form of dislocation dissociation has been observed. The computer simulations have shown why the temperature dependence of the flow strength is so distinct at low temperatures and why the DO_{22} form is always so brittle.

20. DISTRIBUTION/AVAILABILITY OF ABSTRACT	21. ABSTRACT SECURITY CLASSIFICATION
UNCLASSIFIED/UNLIMITED ☒ SAME AS RPT. ☐ DTIC USERS ☐	UNCLASSIFIED

22a. NAME OF RESPONSIBLE INDIVIDUAL	22b. TELEPHONE NUMBER (Include Area Code)	22c. OFFICE SYMBOL
~~David Pope~~ Rosenstein	202-767-4933	NE

DD FORM 1473, 83 APR EDITION OF 1 JAN 73 IS OBSOLETE.

SECURITY CLASSIFICATION OF THIS PAGE

PLASTICITY OF SINGLE CRYSTALLINE AL_3X INTERMETALLIC COMPOUNDS

V. Vitek, D. P. Pope and D. E. Luzzi
Department of materials Science and Engineering, University of Pennsylvania, Philadelphia, PA 19104

Deformation behavior of $L1_2$ Al_3Ti-Fe

Titanium rods, aluminum buttons and iron flakes of high purity were first melted in a crucible in an induction furnace under an argon atmosphere, then cast into a copper mold to form a 220g rod with nominal composition $Al_{66}Ti_{28}Fe_6$. Weight loss during the melting was negligible. Part of the rod was pulverized, then placed into an alumina crucible of 2.2 cm diameter and 60 degree tip angle. A single crystal was grown using the modified Bridgman method as described by Wee, Pope and Vitek (1984). The samples for mechanical testing were annealed at 1100 °C for 60 h in vacuum and cooled slowly at a rate about 65 °C/h to ambient temperature. The distribution and composition of phases in the crystal were checked using X-ray powder diffraction and quantitative energy dispersive spectroscopy in an SEM. Specimens of dimension 3x3x5 mm with compressive axes near [001], [013], [113], [112] and [133] were prepared in the same way as described elsewhere (Wu et al. 1990a). Compression tests were performed on an Instron Universal Testing Machine at a nominal strain rate of about $1.7x10^{-4}$ s^{-1} at temperatures between 77K and 1300K. Operating slip systems were identified using two-surface slip trace analysis on a metallurgical microscope equipped with Nomarski interference contrast.

The as-grown crystal is of overall composition $Al_{66.8}Ti_{27.4}Fe_{5.8}$ and consists of an $L1_2$ matrix and some Al_2Ti (actual chemical composition is $Al_{65.8}Ti_{33.7}Fe_{0.5}$) and a smaller amount of $AlTi_3$ (actual composition is $Al_{33.5}Ti_{66.5}$ which is in the $AlTi_3$ phase field (Massalski et. al. (1986)). The Al_2Ti is apparently coherent with the matrix and forms epitaxially on the cube planes of the matrix as shown in Fig. 1. The amount and distribution of Al_2Ti depends on the heat treatment: it appears if the crystal is cooled slowly to the ambient temperature from 1100°C, but disappears if the specimen is reheated to 1200 °C for 2h and quenched in water. This clearly indicates that the single $L1_2$ phase field is larger at 1200°C than at

lower temperatures. The result is consistent with the Al-Ti-Fe ternary isotherm determined by Mazdiyasni et. al. (1989), in which the $L1_2$ single phase field is found to be larger at 1200 °C than at 800 °C. The appearance of Al_2Ti in the slowly cooled sample suggests that the single phase field is smaller still at lower temperatures.

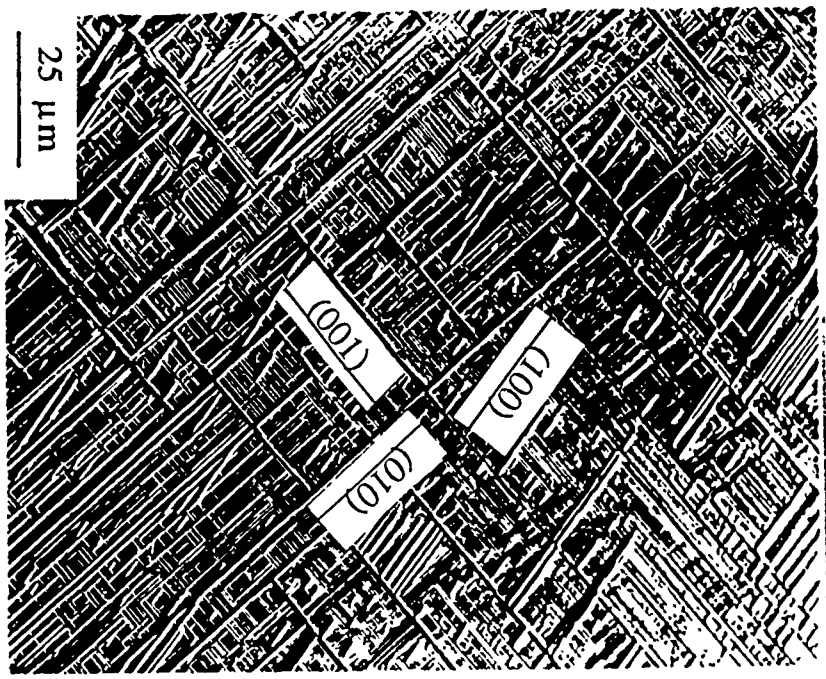

Fig.1 The morphology of a single crystalline specimen. Note that the Al_2Ti phase grew epitaxially on the cube planes of the matrix.

There are two types of the shape of the $AlTi_3$ phase when viewed in the cross section: one is more or less rectangular in shape of typical size around 25-40 μm, similar to those previously reported (Wu et. al. 1990a), and the other forms narrow ribbons 0.1-1.5 mm long and 10 μm thick. The ribbons apparently form during solidification since they are continuous throughout the crystal. Even though the $AlTi_3$ constitutes a small volume fraction of the crystal, to the extent that it is not seen in the diffraction patterns, it has a dramatic effect on the fracture behavior. Cracks are often seen near the ribbons, or propagate along the interface between the matrix and the ribbons or within the ribbons themselves. Furthermore, slip lines in the matrix are commonly seen to terminate at the ribbons.

The single crystal was found to be much more brittle than the polycrystal. Figure 2 shows a fractured single crystalline sample tested at a strain rate about $1.7x10^{-3}$ s^{-1} at 770°C. Although three octahedral and one cube slip systems were activated near the fracture surfaces, the specimen failed in a brittle manner. The failure occurred by cleavage on {110}, {001}, {013} and {111} planes. The observation agrees well with the results reported by George et al. (1990) based on their study of Al_3Ti alloy modified by Fe. The operating slip systems seen in the specimens with compressive axes near [001], [112], [013] and [133], tested at elevated temperatures, were analyzed (Fig.3). In the specimens with compressive axes near-[001] and -[013], the operating slip systems at all temperatures are predominantly octahedral, although some cube slip lines were seen at high temperatures. For these two orientations the Schmid factor for cube slip is substantially smaller than for octahedral slip. In specimens orientated near [112] and [133], the Schmid factors for cube and octahedral slip are comparable; however, only octahedral slip was observed at low temperatures. As the temperature was increased, both octahedral and cube slip were activated, and in the near-[133] specimen the number of cube slip lines observed at high temperatures exceeded the number of octahedral slip lines (Fig.3). The change of the slip system from octahedral to cube as the temperature is increased, and as the compressive axis is moved from [001] towards [111] in the standard unit triangle, is also observed in the Ni_3Al (Lall et.al. 1979). However, the change seen here is much more gradual than in Ni_3Al.

TABLE I.

Schmid Factors for the Specimens Tested

Orientation	[101](111)	[101](111)	[011](111)	[110](001)	[101](010)
1	0.476	0.463	0.405	0.199	0.158
2	0.482	0.436	0.410	0.323	0.242
3	0.483	0.418	0.390	0.373	0.292
4	0.497	0.473	0.349	0.288	0.252
5	0.445	0.326	0.162	0.447	0.437
6	0.461	0.360	0.385	0.433	0.340

Figures 4a and b show the flow behavior and corresponding CRSS as functions of temperature and orientation. Generally the yield stress and the CRSS are

relatively constant in the intermediate temperature range (very much plateau-like), but increase rapidly at low and decrease rapidly at high temperatures. The sharp increase of the yield stress as temperature is decreased has also been seen by Wee et al. (1984) in $L1_2$ Pt_3Al. This flow behavior can be attributed to the sessile nature of screw dislocations due to a non-planar core configuration as discussed in the section dealing with the theoretical analysis.

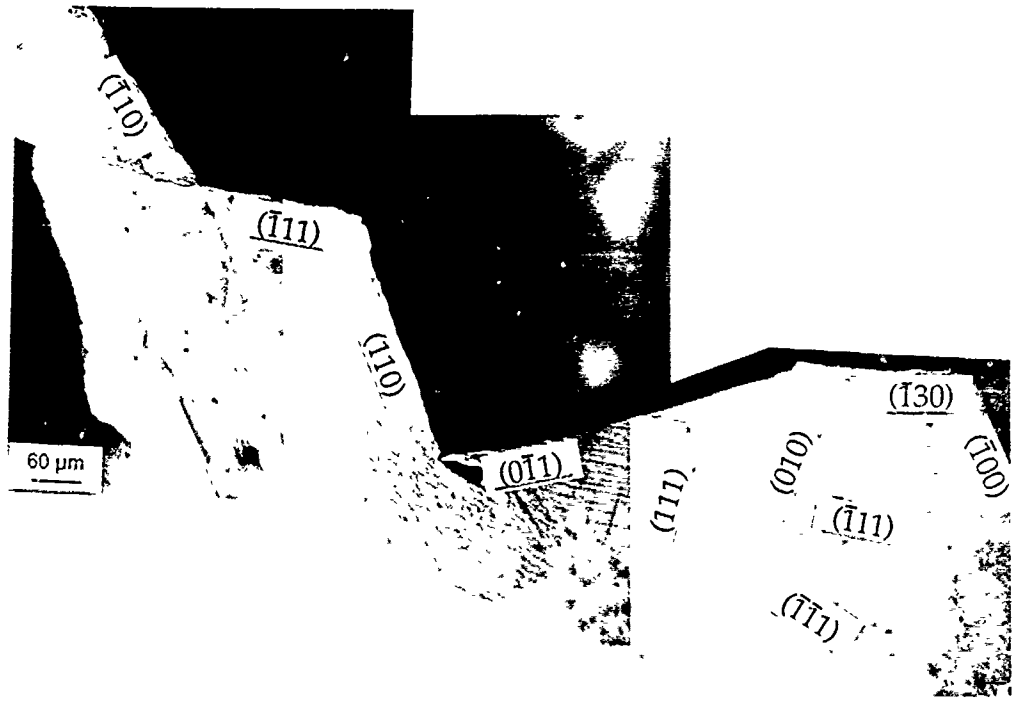

Fig. 2. A specimen broken at 770°C by cleavage on {011}, {001}, {013} and {111} planes as indicated.

The yield stress of $Al_{66.8}Ti_{27.4}Fe_{5.8}$ is lower than that of $Al_{63.7}Ti_{28.7}Fe_{7.6}$ but much higher than that of $Al_{64.6}Ti_{25.7}Fe_{9.7}$, see Wu et. al. (1990a,b) for comparison. The yield stress has a very strong dependence on Ti content, the higher the Ti content, the higher the yield stress. Also, the yield stress shows an increase with increasing amounts of Fe substituting for Al. In all cases we cannot absolutely rule out the existence of a finely divided second phase that gives rise to the strong compositional dependence of the flow stress. Only the $Al_{66.8}Ti_{27.4}Fe_{5.8}$ was examined in TEM and in this material if small particles exist they must be smaller than 300 Å. Since the $Al_{63.7}Ti_{28.7}Fe_{7.6}$ and $Al_{64.6}Ti_{25.7}Fe_{9.7}$ were

examined only with optical microscopy and SEM, such particles, if they exist, could be larger.

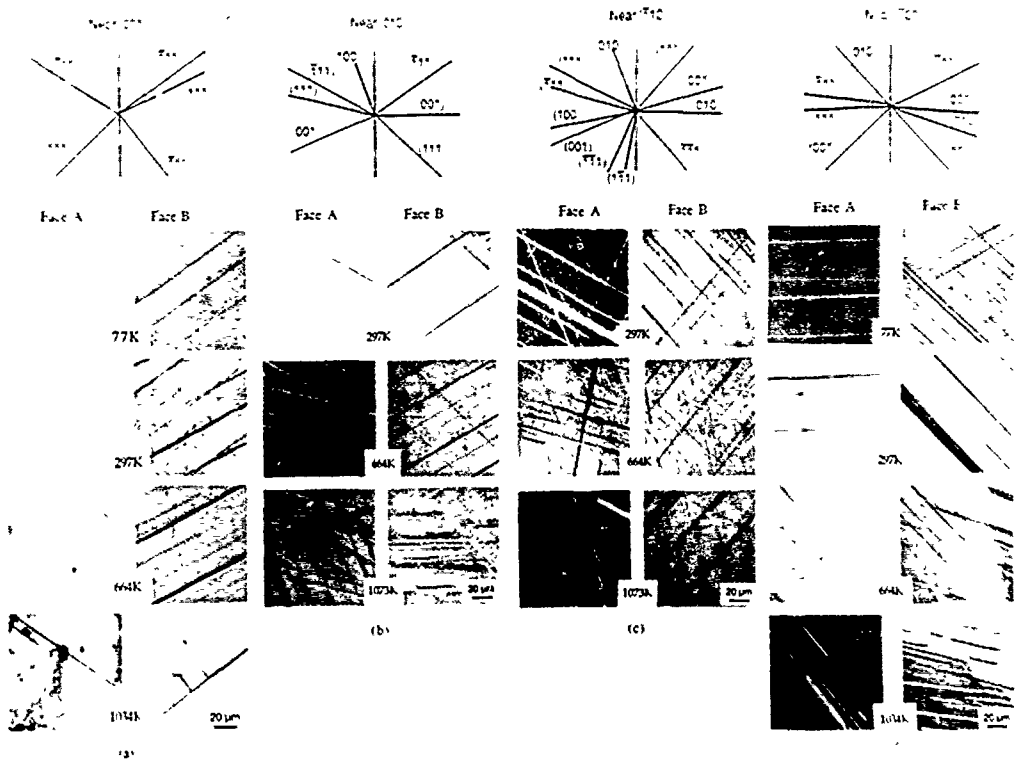

Fig. 3. Slip traces seen on two orthogonal surfaces of specimens: (a) near-[001], (b)near-[013], (c) near-[112] and (d) near-[133].

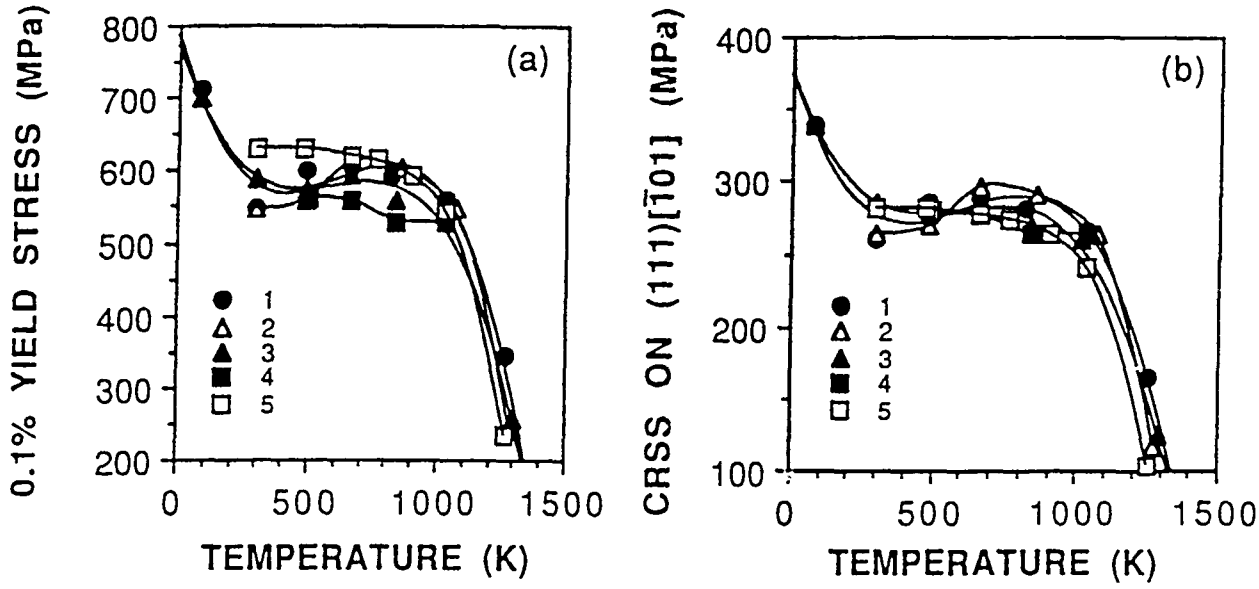

Fig. 4. Temperature dependence of (a) the axial yield stress of single crystal specimens, and (b) corresponding critical resolved shear stress resolved onto the (111)[101] slip system.

Transmission electron microscopy of dislocations

To understand the deformation mechanisms and related causes of possible brittleness in a particular alloy, it is always necessary to know the slip systems and the nature of dislocation dissociations (Vitek 1984, Veyssiere 1988, Duesbery 1989). However, until the present effort, no single crystal experiments designed to determine the operating slip systems had been done and only very limited transmission electron microscopy (TEM) studies of the dislocation structures in Al_3Ti and other trialuminides had been made. In our research, we investigate by means of high resolution weak beam transmission electron microscopy dislocation structures and dissociation modes of <110> superdislocations in $Al_{67}Fe_8Ti_{25}$ and $Al_{66}Fe_6Ti_{23}V_5$ alloys deformed at room temperature and 600°C, respectively. These two temperatures correspond to the low and high temperature deformation regimes described in the previous section. However, since no significant

differences in the dislocation structures and dissociations were observed for these two alloys, only the results obtained for $Al_{67}Fe_8Ti_{25}$ are described in detail.

Alloys of nominal composition $Al_{67}Fe_8Ti_{25}$ and $Al_{66}Fe_6Ti_{23}V_5$ were obtained from Oak Ridge National Laboratory through collaboration with Dr. W. Porter. These alloys had been produced by arc melting followed by extrusion at 1100°C to a diameter of 10 mm while encased in a stainless steel pipe. Pieces 32 mm long were cut from the rod and placed under a compressive load at room temperature until plastic strains of 1.5% ($Al_{67}Fe_8Ti_{25}$) and 3.0% ($Al_{66}Fe_6Ti_{23}V_5$) were attained. This as-received material had a grain size of approximately 10 to 20 mm and contained a small amount of secondary phases (mostly oxides) at grain boundaries. Several test pieces, measuring approximately 2 mm x 2 mm x 6 mm, were cut from the as-received material and deformed under compression at 600 C with a strain rate of about 10^{-4} s^{-1} until an additional 5% plastic strain was reached. Slices were cut from the deformed samples using an electric discharge machine and were mechanically polished to 100 microns in thickness. Final preparation for TEM observation was accomplished by jet-polishing at -45°C using a solution of perchloric acid, n-butyl alcohol and methanol (5:25:75 in volume). The dislocation structures of the as-received and the subsequently compressed samples were observed by a Philips EM-400 electron microscope operated at 120 kV, employing both the bright-field (BF) and dark-field weak-beam imaging techniques.

Room Temperature Deformation

Slip plane analysis in the TEM specimens indicated that {111} octahedral slip occurs in the low temperature regime in the $Al_{67}Fe_8Ti_{25}$ alloy, in agreement with the single crystal experiments. The dislocations found in samples deformed at room temperature show a strong tendency to form dipoles. Most importantly, it was found that superdislocations with total Burgers vector a<110> dissociated into two 1/3<112> superpartials separated by superlattice intrinsic stacking faults (SISFs) on {111} planes. The TEM analysis of this type of dissociation is quite difficult since the separation of the superpartials is small. However, the signature of the SISF will be fringing localized to the superdislocation seen in weak beam images in which the contrast of the superpartials is weak. An example of the fringing is shown in Fig. 5. In this figure, several dislocations can be seen in a strong contrast condition. Near these dislocations a faint fringing can be seen

which is the signature of the SISF. A measurement of the separation of the superpartial dislocations gave a value of 5 ± 1 nm at room temperature giving an estimated value of the stacking fault energy of 100 mJ/m^2.

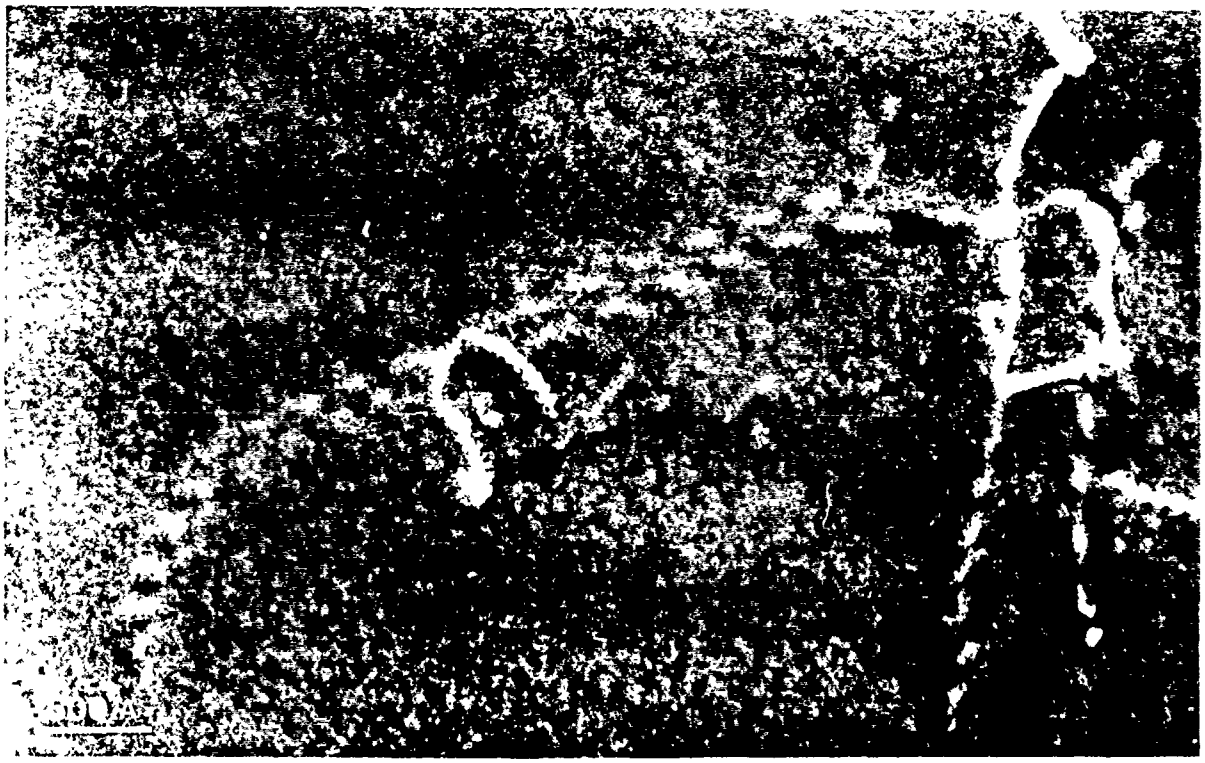

Fig. 5. Weak beam image used to determine the configuration of the dissociated superdislocations formed during room temperature deformation. Fringing from the SISF can be seen, indicating that the dissociation is into two 1/3<112> superpartials.

600°C Deformation

Dislocations, predominantly with near-edge character, dissociated into two 1/2<110> superpartials separated by antiphase boundaries (APBs) on the cube {001} planes, were observed in samples deformed at 600°C. The separation of the superpartials in this case was much more extensive, approximately 15 nm. Using

this value, the APB energy on the {001} planes is approximately 100mJ/m^2. The confirmation that the <110> superdislocations dissociate into 1/2<110> superpartials was obtained by observing the contrast of the superpartials as a function of imaging condition and by dark field imaging using a superlattice reflection which originates from the chemical ordering. Bright contrast along the superdislocations in the dark field images confirmed the presence of the APB between the superpartials. Tilting experiments in which the separation of the superpartials was monitored as a function of specimen orientation was used to determine the dissociation plane. The observation of the widest separation when the electron beam was perpendicular to the {001} cube plane indicated that this was the dissociation plane. The sequence of images is shown in Fig. 6.

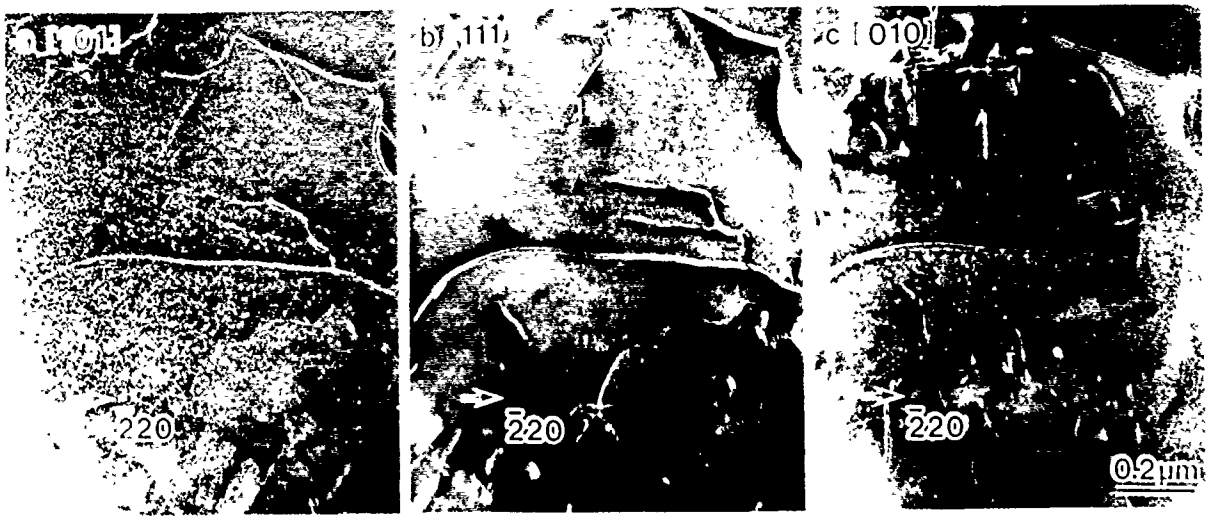

Fig. 6. Weak beam images of a<110> superdislocation formed during 600°C deformation viewed in different orientations with the same operating reflection (-220). (a) [110], (b) [111], (c) [001]. It can be seen from the separation of the partial dislocations that the superdislocation is dissociated on the cube plane.

Theoretical analysis of the dislocation core structures and relation to low temperature plastic behavior

Al_3Ti in Ll_2 form

The temperature dependence of the yield stress observed in the Ll_2-modified Al_3Ti is very different from that of the compounds like Ni_3Al, but it is very similar to that observed in a number of platinum based $L1_2$ compounds, in particular Pt_3Al (Yadogawa, Wee, Oya and Suzuki, 1980; Wee, Pope and V. Vitek,1984; Heredia, Tichy, Pope and Vitek, 1989). In this alloy both the {111} and {001} slip planes were observed, depending on the orientation of the sample. The temperature and orientation dependences of the yield stress were then explained by very similar sessile cores of 1/3<112> superpartials on {111} planes and 1/2<110> superpartials on {001} planes. The reason why the 1/3<112> and not 1/2<110> superpartials on {111} planes play the primary role is that the APB on {111} plane is either unstable or has such a high energy that the dissociation involving this APB cannot occur. In Al_3Ti the observed slip system at low temperatures is <110> {111} and since the temperature dependence of the yield stress is similar as in Pt_3Al it is likely that the <110> dislocations are dissociated into 1/3<112> superpartials the cores of which are again sessile. This is, indeed, supported by the weak-beam electron microscope observations, as described above.

In order to investigate such situation a model many-body potential leading to a very high APB energy on {111} planes and an unstable CSF has been constructed. Using this potential the core structure of the 1/3[1$\bar{2}$1] superpartial bounding the SISF on the (111) plane has been calculated. The result is shown in Fig. 7. This superpartial possesses an edge component, but only the screw ([1$\bar{1}$0]) component of the displacements is shown here. In this and the following figures the atomic arrangement is shown in the projection perpendicular to the direction of the dislocation line ([1$\bar{1}$0]). Small circles represent the A atoms, and large circles the B atoms of the A_3B alloy. Two consecutive crystal planes ((2$\bar{2}$0)) are always shown and distinguished as darkly and lightly shaded circles. The screw ([1$\bar{1}$0]) components of the relative displacements of the neighboring atoms are represented by the arrows the length of which is proportional to the magnitude of the displacement and normalized by the magnitude of the Burgers vector (| 1/2[1$\bar{1}$))0] |). The rows of arrows of constant length represent the SISF.

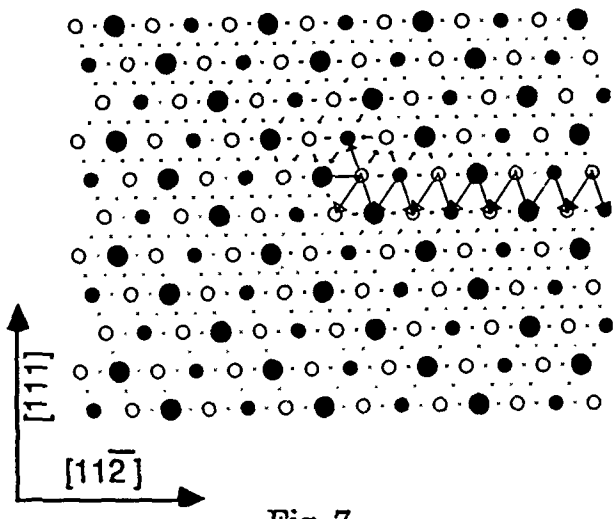

Fig. 7.

1/3[1$\bar{2}$1] superpartial in the model material bounding the SISF on the (111) plane.

It is seen from Fig. 7 that the screw displacements are spread simultaneously into the (111) plane, one layer above the plane of the SISF, and to the (1$\bar{1}$1) plane. However, the edge component is spread in the plane of the fault. This core structure is shown schematically in Fig. 8. The non-planar spreading of the dislocation core suggests that the Peierls stress of such dislocations is very

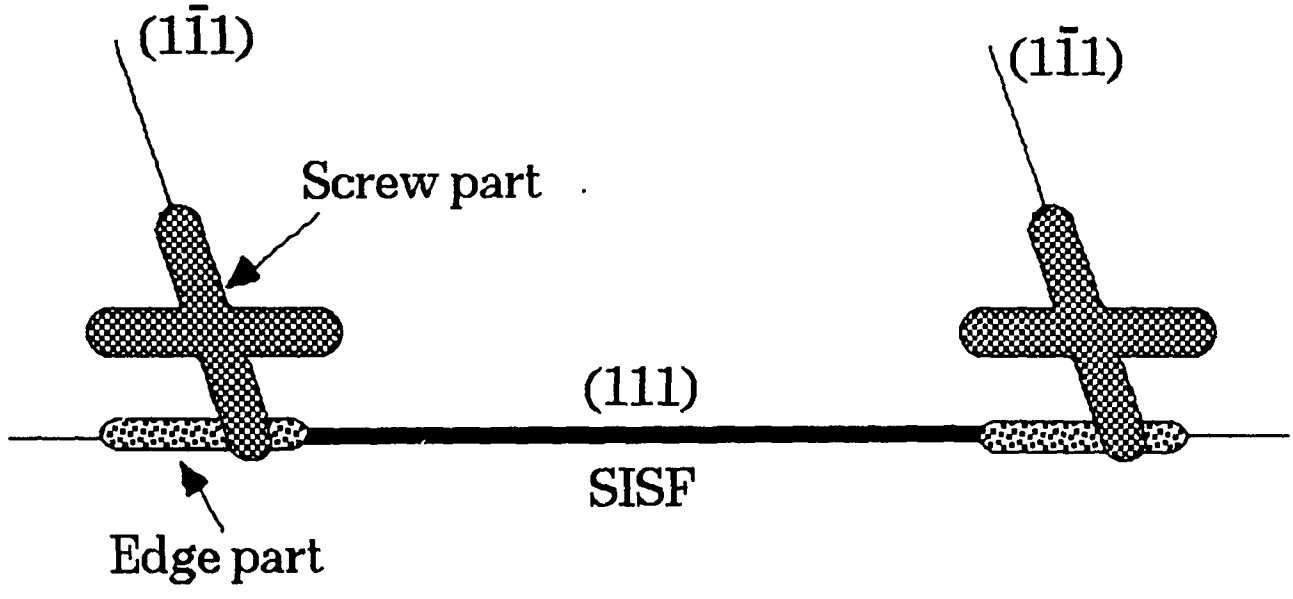

Fig. 8. The schematic picture of the cores of the superpartials forming the dislocation dissociated according to the reaction 1/2[1$\bar{1}$0] = 1/3[1$\bar{2}$1] + 1/3[2$\bar{1}\bar{1}$].

high. This has, indeed, been tested by simulating the motion of such dislocations under the effect of the applied stress. The dislocation shown in Fig. 7 starts to glidealong the (111) plane when the applied shear stress in this plane in the [1$\bar{1}$0] direction is 0.03G, where G is the shear modulus. On the other hand, only a stress

of 0.005G is needed for the glide of the $1/2[1\bar{1}0]$ dislocations in Ni_3Al which bound the APB on the (111) plane and possess a planar core. However, the motion of sessile dislocations can be aided by thermal activations and thus the yield stress will be increasing rapidly with decreasing temperature. A theory of the temperature dependence of the yield stress in such compounds was developed in Tichy, Vitek and Pope, 1986). The sessile form of the dislocation cores in Al_3Ti makes the dislocations less mobile than in materials such as Ni_3Al and causes a strong temperature dependence of the flow stress. This behavior is analogous to that observed in b.c.c. metals which are usually ductile, at least at high temperatures. Similarly, Al_3Ti can also be ductile, in particular at high temperatures, as observed. Hence, the sessile nature of the screw dislocations leads to a relatively high and temperature dependent yield stress but cannot be solely responsible for the extreme brittleness of this material when loaded in tension.

Al_3Ti in DO_{22} form

In the stoichiometric form Al_3Ti crystalizes in the tetragonal DO_{22} structure. It is then commonly assumed that in this structure there are not enough available slip systems, therefore, it is natural that this material is brittle. However, there are two types of perfect superdislocations with Burgers vectors of very similar magnitude, $[1\bar{1}0]$ and $1/2[11\bar{2}]$. (For simplicity, we use the f.c.c. notation for the Miller indices with the third index referring to the c-axis of the tetragonal cell). The former can slip on (111) and (001) planes while the latter on (111) planes. In the DO_{22} structure there are four equivalent {111} planes each containing one <110> type and one <112> type vector; there is one (001) plane containing two <110> type vectors. Hence, there are ten available slip systems in the DO_{22} structure and it is not, therefore, a priori clear that a DO_{22} compound cannot be ductile.

It is possible, however, that a consequence of the tetragonal structure is that the cores of these dislocations are not glissile and the dislocations are, therefore. difficult to move. In order to investigate the core phenomena we have constructed a model many-body potential (Khantha, Vitek and Pope,1991) such that the elastic constants and the c/a ratio are similar to those found for Al_3Ti in recent ab-initio electronic structure calculations (Fu, 1990).

The superdislocations with Burgers vectors $[1\bar{1}0]$ can dissociate in the DO_{22} structure on both (111) and (001) planes into $1/2[1\bar{1}0]$ superpartials with the APB in between them. The core structure of the $1/2[1\bar{1}0]$ superpartial bounding the APB on the (111) plane is shown in Fig. 9a using the same type of display as above and, schematically, in Fig. 9b. The characteristic feature is the spread of thedislocation core into the $(11\bar{1})$ plane along the [112] direction which can be interpreted as dissociation into 1/6<112> type partials with the CSF in between them. Figs. 10a and 10b show the core configuration of the $1/2\ [1\bar{1}0]$ superpartial bounding the APB on the (0 0 1) plane. The core is now spread on both (1 1 1) and (1 1 $\bar{1}$) planes. Thus the core of the 1/2<110> superpartials is always sessile, whether the corresponding APB is on {111} or {001} planes.

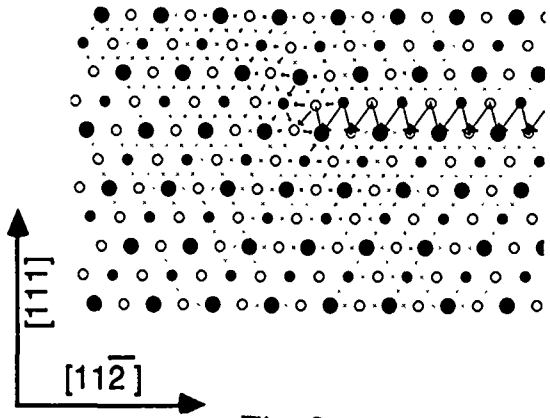

Fig. 9a.
The core configuration of the $1/2[1\bar{1}0]$ superpartial in the model DO_{22} material bounding the APB on the (111) plane.

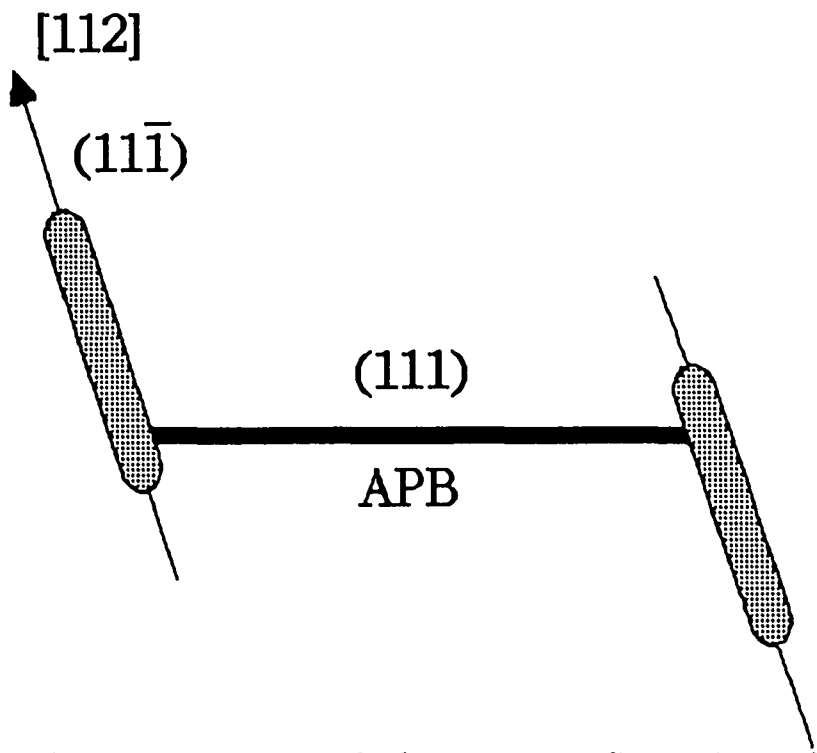

Fig. 9b. The schematic picture of the core configuration of the $[1\bar{1}0]$ superdislocation in the model DO_{22} dissociated on the (111) plane into $1/2\ [1\bar{1}0]$ superpartials.

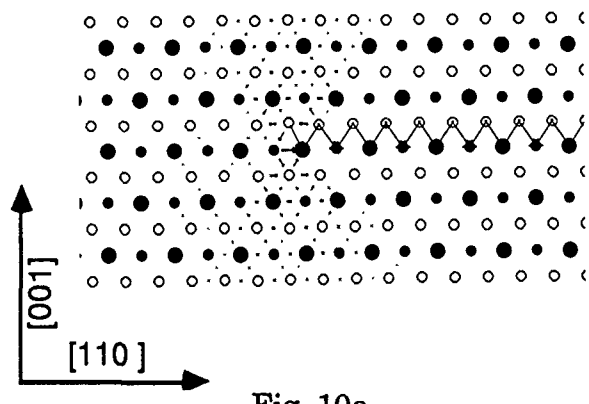

Fig. 10a
The core structure of the 1/2[1$\bar{1}$0] superpartial in the model DO_{22} material bounding the APB on the (001) plane.

The 1/2[11$\bar{2}$] superdislocation may dissociate on the (111) plane into the superpartials 1/6[11$\bar{2}$] and 1/3[11$\bar{2}$] separated by the SISF. However, owing to the elastic anisotropy the energy of the dissociated 1/2[11$\bar{2}$] dislocation is lower than that of the [1$\bar{1}$0] dislocation only if the SISF energy is much lower than the APB energy. The core structure of both the 1/6[11$\bar{2}$] and 1/3[11$\bar{2}$] superpartials was calculated. In the former case the core is planar spread in the plane of the SISF but in

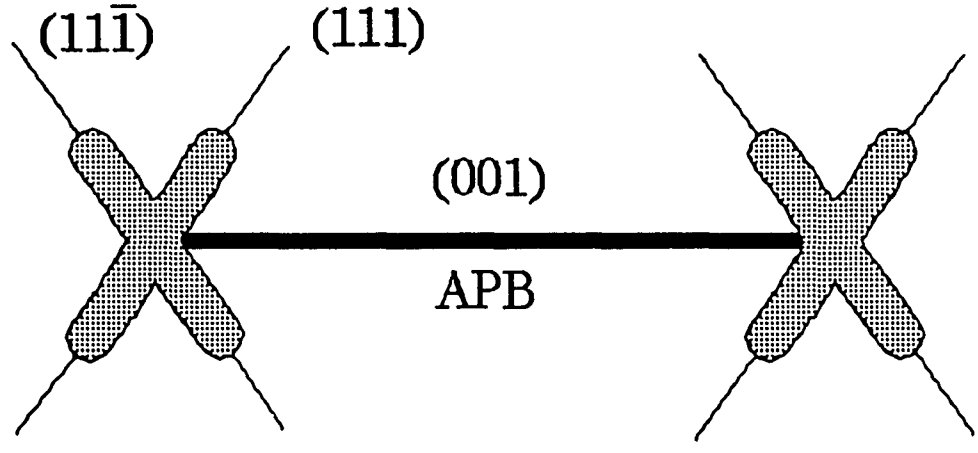

Fig. 10b. The schematic picture of the core configuration of the [1$\bar{1}$0] superdislocation in the model DO_{22} dissociated on the (001) plane into 1/2 [1$\bar{1}$0] superpartials.

the latter case the core has a zonal character and spreads into three parallel (111) planes. This core spreading may render the 1/3[11$\bar{2}$] superpartial sessile but this problem is being studied at present.

These results suggest that in the DO_{22} compounds the available dislocations are all sessile in the screw orientation and thus it is not only the lack of slip systems but also the sessile nature of dislocations which renders these alloys

rather brittle. The thermally activated motion of sessile dislocations is, of course, possible and <110> slip has, indeed, been observed at high temperatures in Al_3V and Al_3Ti (Williams and Blackburn, 1970; Yamaguchi, Umakoshi and Yamane, 1987). In the former case the yield stress increases rapidly with decreasing temperature, as expected. However, in the latter case the major mode of deformation is twinning of the type $(111)[11\bar{2}]$ which can be regarded as produced by the motion of $(1/6)[11\bar{2}]$ superpartials on successive (111) planes. The above mentioned calculations show that these dislocations possess planar cores and are thus mobile. Hence, unlike in the case of slip, the motion of twinning dislocations is not hindered by their core structure.

References

Duesbery, M. S., 1989, *Dislocations in Solids*, edited by F. R. N. Nabarro (Elsevier: Amsterdam), p. 67.

Fu, C.L., 1990, J. Mater. Res. **5**, 971.

George, E.P., Horton, J.A., Porter, W.D. and Schneibel, J.H., 1990, *J. Mater. Res.*, **5**, 1639.

Heredia, F. E., Tichy, G., Pope, D. P. and Vitek, V., 1989, *Acta Metall.* **37**, 2755.

Khantha, M., Vitek, V. and Pope, D. P., 1991, *High Temperature Ordered Intermetallic Alloys IV*, edited by L. Johnson, J. O. Stiegler and D.P. Pope, MRS Symposium Proceedings, in press .

Lall, C., Chin, S. and Pope, D.P., 1979, *Met. Trans.*, **10A**, 1323.

Massalski, T.B., Murray, J., Bennett, L.H. and Baker, K., 1986, *Binary Alloy Phase Diagrams*, (American Society for Metals, Metals Park, Ohio), p. 175.

Mazdiyasni, S., Miracle, D.B., Dimiduk, D.M., Mendiratta, M.G. and Subramanian, P.R., 1989, *Scripta Metall.*, **23**, 327.

Tichy, G., Vitek, V. and Pope, D. P., 1986, *Phil. Mag. A* **53**, 485 .

Veyssiere, P., 1988, *Rev. Phys. Appl. Paris* **23**, 673.

Vitek, V., 1985, *Dislocations and Properties of Real Materials*, edited by M. H. Loretto (The Institute of Metals: London), p. 30.

Wee, D. M., Pope D. P. and Vitek, V., 1984, *Acta Metall.* **32**, 829.

Williams, J. C. and Blackburn, M. J., 1970, *Ordered Alloys: Structural Applications and Physical Metallurgy*, edited by B. H. Kear, T. Sims, S. Stoloff and J. H. Westbrook, p. 425.

Yadogawa, M. , Wee, D. M., Oya, Y. and Suzuki, T., 1980, *Scripta Metall.* **14**, 849.
Yamaguchi, M., Umakoshi, Y. and Yamane, T., 1987, *Phil. Mag.* A **55**, 301.
Wu, Z.L., Pope, D.P. and Vitek, V., 1990a, *Scripta Metall.* **24**, 2187; 1990b, ibid. 2191.